RSC Advances

ROYAL SOCIETY OF CHEMISTRY

www.rsc.org/advances

Journal Name

ARTICLE

Melt-compounded polylactic acid composite hybrids with hydroxyapatite nanorods and silver nanoparticles: Biodegradation, antibacterial ability, bioactivity and cytotoxicity

Chen Liu[a], Kai Wang Chan[a], Jie Shen[b], Hoi Man Wong[b], Kelvin Wai Kwok Yeung[b] and Sie Chin Tjong[a]*

Designing bulk polymer composite materials with firmly embedded nanofillers having good biocompatibility, high bactericidal activity and large scale production capability is considered of technological importance. Biodegradable polylactic acid (PLA) with 18 wt% hydroxyapatite nanorod (nHA) and silver nanoparticle (AgNP) of different loadings were fabricated by melt-compounding process. Hybridizing nHA with AgNP fillers in the PLA matrix permitted efficient attachment and proliferation of osteoblasts and good bactericidal ability of the resulting nanocomposites. This study aimed to evaluate the biodegradation, antibacterial ability, bioactivity and cytotoxicity of melt-compounded PLA/18%nHA-Ag hybrids using solution immersion, water contact angle, agar disk diffusion, 3-(4,5-dimethylthiazol-2-yl)-2,5-diphenyltetrazolium bromide (MTT) assay and biomineralization measurements. Weight-loss and water contact angle measurements showed that the nHA and Ag nanofillers increase the degradation rate and hydrophilicity of PLA, respectively; AgNPs were more effective than nHA for those tests. Disk diffusion test results demonstrated that the PLA/18%nHA-Ag hybrids show high bactericidal activity against Escherichia coli and moderate activity against staphylococcus aureus. MTT test results revealed that high AgNP contents (18 and 25 wt%) in the PLA hybrids inhibit the proliferation of osteoblasts. However, composite hybrids with low loading Ag levels (2 and 6 wt%) showed good biocompatibility. Such hybrids maintained a good balance between antibacterial activity and cytocompatibility. Biomineralization test revealed that a dense apatite layer can be fully developed on the surfaces of PLA/18%nHA-Ag hybrids. The development of industrially scalable, efficient and cost effective polymer composite hybrids with good osteoconductivity and great bactericidal activity opens new perspective for bone tissue engineering applications.

a. *Department of Physics and Materials Science, City University of Hong Kong, Tat Chee Avenue, Kowloon, Hong Kong*

b. *Department of Orthopedics and Traumatology, Li Ka Shing Faculty of Medicine, The University of Hong Kong, Hong Kong*

Introduction

Synthetic polymers have been widely employed as biomaterials for making medical devices and tissue engineering scaffolds since they exhibit attractive properties such as lightweight, good processability, mechanical flexibility and degradable behavior.

(certain biodegradable polymers).[1-7] The advantages of synthetic over natural biodegradable polymers include mass production capability, tailored mechanical behavior and degradation rate to meet biomedical applications. Biopolymers such as polylactic acid (PLA), poly(caprolactone) and polyglycolic acid degrade over time in human body during which the tissue is growing, thus the need for a revision surgery to remove the implant is eliminated.[8-13] The chemical structures of these polymers allow hydrolytic degradation through de-esterification. These synthetic biopolymers can also be made into different shapes and structures. Typical examples are scaffolds, plates, screws, pins and fixation devices.[14,15]

Polymers generally have low elastic modulus and strength comparing with metals. Their tensile properties can be improved by adding fillers of micrometer sizes.[16-21] Therefore, the composite approach appears to be very effective for fabricating polymer biomaterials with desired mechanical properties. Conventional polymer composites require large filler volume fractions to attain designed physical and mechanical properties. This leads to low mechanical strength and poor processability of the resulting materials. Moreover, deleterious stress shielding effect arising from the use of high-modulus metallic implants has led to increased research into the development of polymer–ceramic composite materials with good biocompatibility. For example, Bonfield and coworkers incorporated 40 vol% hydroxyapatite microparticles to high-density polyethylene to form HAPEX^{TM} composite.[22] Synthetic hydroxyapatite [$Ca_{10}(PO_4)_6(OH)_2$)] resembles mineral component of human bones and provides structural support for bones. The addition of hydroxyapatite microparticles (mHA) can enhance biocompatibility of polyethylene. However, large mHA usually debond from the polymer matrix of microcomposites during the tensile test, causing low tensile strength accordingly.[23] For biodegradable polymers, large mHA loading levels have also been added to form composites. [24-25] The tensile strength of such composites decrease considerably with increasing mHA content from 20 to 50 wt%.[25]

Nanotechnology brings innovation to the development and synthesis of advanced materials with functional properties at nanometer level. Nanomaterials exhibit improved mechanical properties and biocompatibility than their micro-counterparts.[26] As a result, only low loading levels of nanomaterials are needed to reinforce polymers to form nanocomposite materials.[27-29] In recent years, the use of nanomaterials in biomedical engineering and orthopedic sectors is rapidly growing due to their potential applications in antimicrobial, bioimaging, drug delivery and bone replacement.[30,31] Bone tissues are known to be composed of nanohydroxyapatite platelets and collagen fibers. Accordingly, synthetic hydroxyapatite nanorod (nHA) can be used as reinforcing fillers for improving bioactivity, biocompatibility and mechanical strength of polymers.[32-34] This is due to well-dispersed nHA with a high surface area to volume ratio in the polymer matrix enhances protein-material interactions of biological cells greatly.[35] Biodegradable polymers generally decomposes into acidic monomers that may cause inflammatory and allergic reactions.[36] Nanohydroxyapatite fillers neutralize the degraded acidic components of biopolymers, thereby improving its osteoconductivity and biocompatibility.[37]

Bacteria and microorganisms often attach to the surfaces of medical implant materials and develop biofilms. Bacteria contamination of medical devices leads to infection risks with high morbidity and mortality. It also results in complications and implantation failures.[38] These issues motivates chemists and materials scientists to develop novel biomaterials and device designs to minimize bacterial infection. Biomaterials incorporated with antibacterial agents such as silver, gold and zinc oxide particles have been extensively studied in recent years.[39-43] Silver-based antimicrobial materials are particular attractive due to silver has strong biocidal effects on numerous species of bacteria. Such materials can avoid biofilm growth and prevent bacterial colonization on their surfaces. Metallic silver is typically inert and nonreactive. In aqueous solutions, silver ion (Ag+) is released, so this cation can interact with proteins and enzymes of bacteria. This causes the destruction of bacteria cell membrane and ultimately leads to cell death. Silver nanoparticles (AgNPs) with high surface area-to volume ratio

facilitate more effective release of silver ions, thus increasing bactericidal activity.[44-46]

From the literature, Ag-HA coatings with good antimicrobial activity for underlying Ti-based alloys has been prepared by magnetron sputtering and electrodeposition methods.[47-49] It is desirable to prepare bulk polymer nanocomposites containing nHA and AgNP hybrid fillers for bone tissue engineering and medical device applications with great bactericidal activity and good osteoconductivity. Recently, Shameli et al. prepared binary PLA/Ag nanocomposite films with 8-32 wt% AgNP using solvent casting method.[50] They reported that the antibacterial activity of PLA/Ag films increases with increasing AgNP content. However, their composite films lack the nHA component acting as the sites for the adhesion and growth of osteoblasts. Further, solution casting can only fabricate composite materials in small quantities, and the use of solvents in the process may cause environmental and health hazards. Mostafa et al. carried out preliminary study on the structure and bioactivity of solution-mixed polyvinylpyrrolidone with nHA and AgNP fillers. They found that silver-doped nanohydroxyapatite improves the bioactivity of the apatite upon immersion in a simulated body fluid solution.[51] Sobczak-Kupiec et al. prepared poly(acrylic acid)/gelatin composites with HA and AgNP fillers using polymerization process. The structural feature of such composites was studied using X-ray diffraction technique.[52] However, the bactericidal activity of the composites was not performed and reported. The aims of this work are to fabricate biodegradable PLA nanocomposites with nHA and AgNP hybrid fillers using melt-compounding processes, and to study antibacterial ability, bioactivity and biocompatibility of hybrid nanocomposites. Fabrication of polymer nanocomposite materials by melt-compounding does not require the use of organic solvents. Moreover, melt-compounding enables mass production of composite products at a low cost. To the best of our knowledge, there is no report in the literature relating the fabrication, antibacterial and cytotoxic properties of biodegradable PLA/nHA-Ag hybrid nanocomposites prepared by melt-mixing.

Experimental

Materials

Nanohydroxyapatite with rod-like appearance was supplied by Nanjing Emperor Nanomaterial (China). Transmission electron microscopy (TEM; Philips CM20) image of nHA revealed that the nanorods exhibit a length of about 100 nm and width of 20 nm (Fig. 1a). Silver nanoparticles and PLA were purchased from Nanostuctured and Amorphous Materials Inc. (Texas, USA), and Shenzhen Bright China Inc. respectively. The mean diameter of AgNPs was determined to be ~60 nm using TEM (Fig. 1b) and SemAfore program. Inorganic reagents like $CaCl_2$, NaCl, KCl, KH_2PO_4, $NaHPO_4$, $NaHCO_3$ and Na_2SO_4 were bought from Sigma Aldrich Inc. (U.S.A.). They were used directly without further purification.
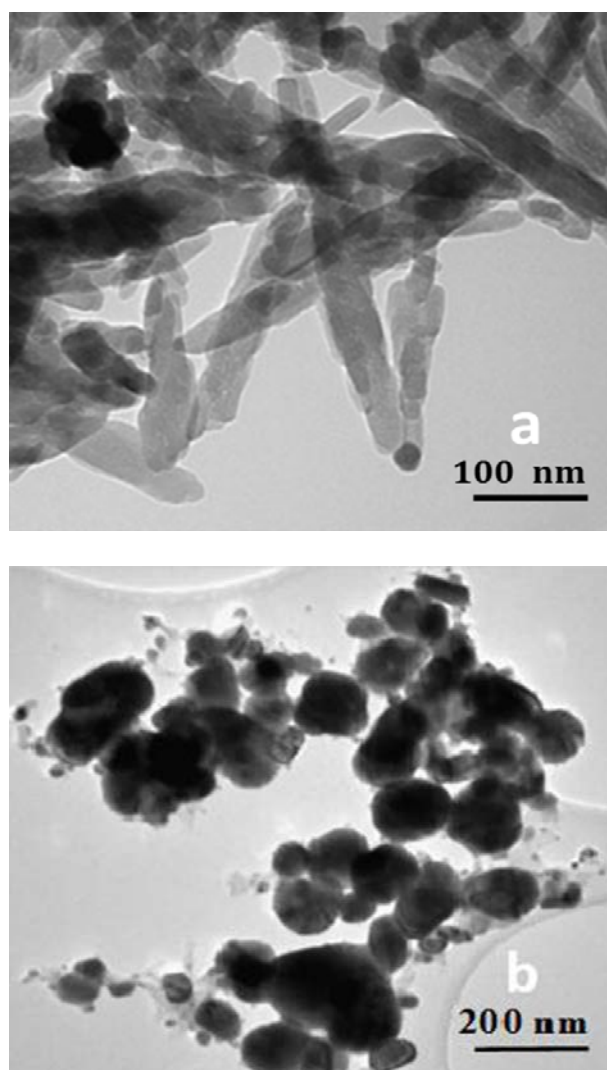

Figure 1. TEM images of (a) nHA rods and (b) silver nanoparticles

ARTICLE

Preparation of nanocomposites

PLA pellets and nHA were dried in an oven at 55°C overnight prior to melt-mixing. Table 1 listed the compositions of hybrid PLA–nHA-Ag composites. For the purpose of comparison, binary PLA/18 wt% nHA nanocomposite was also fabricated. Melt-mixing of these composites were carried out by feeding respective material mixtures into a Haake mixer under a screw rotation speed of 40 rpm at 200 °C for 45 min. Finally, the obtained materials were dried and compression molded with a hot press into thin disks of 2 mm thickness. The specimens for morphological observations were cryo-fractured in liquid nitrogen, then coated with a thin gold layer on their surfaces and placed into SEM (JEOL, JSM 820).

Table 1. Compositions of the nanocomposites studied

Sample	PLA (wt%)	nHA (wt%)	Ag (wt%)
PLA/18% nHA	82	18	0
PLA/18% nHA – 2% Ag	80	18	2
PLA/18% nHA – 6% Ag	76	18	6
PLA/18% nHA – 10% Ag	72	18	10
PLA/18% nHA – 18% Ag	64	18	18
PLA/18% nHA – 25% Ag	57	18	25

XRD analysis

X-ray diffraction (XRD) measurements were performed using a Bruker D2 Phaser X-ray diffractometer (Bruker, U.S.A) with Cu-Kα radiation (λ = 1.5418 nm; 30kV). The patterns were collected in the 2θ range from 10° to 60°.

Silver ion release

Thin disks (10 mm diameter) of binary PLA/18%nHA and hybrid PLA/Ag-nHA nanocomposites were immersed in 10 ml of distilled water for periods ranging from 2 to 50 days at 37 °C. The concentration of silver ions in distilled water was determined with inductively coupled plasma atomic emission spectrometry (ICP-AES; Perkin Elmer 3300DV).

Water contact angle

Deionized water contact angle tests were carried out to evaluate hydrophobic or hydrophilic nature of nanocomposite specimens. The tests were performed by water drops on the flat specimen surfaces using Rame Hart 500-F1 advanced goniometer (Rame-Hart Instrument Co., NJ, USA). The measurements were repeated six times for each material sample.

In vitro degradation

Phosphate buffer saline (PBS) with a pH of 7.4 was prepared by dissolving NaCl, KCl, KH_2PO_4 and Na_2HPO_4 (137mM NaCl, 2.68mM KCl, 2 mM KH_2PO_4, 10 mM Na_2HPO_4) in deionized water. The nanocomposite specimens were weighed initially prior to immersion. They were then dipped into the solution at 37°C according to ASTM standard method F1635-04.[53] At defined time interval, the specimens were taken out from PBS, washed with deionized water, dried and weighed. The degradation of each specimen was evaluated in term of mass loss defining by the following equation,

$$Mass\ loss\ \% = (M_i - M_f) \times 100/M_i \qquad [1]$$

where M_i and M_f were the initial and final mass of the specimen.

Antibacterial tests

The antibacterial activities were assessed against gram-negative *Escherichia coli* (*E. coli*) and gram-positive *Staphylococcus aureus* (*S. aureus*) using Bauer-Kirby disk diffusion method[54,55] The inoculums of *E.coli* and *S. aureus* were prepared in an incubator (37°C, 5% CO_2 in air) from frozen samples with fresh Lysogeny broth (LB) and brain heart infusion (BHI) broth, respectively. Furthermore, 0.1M $AgNO_3$ was used as positive control and pure PLA was treated as negative control.

The disk diffusion test was carried out by pouring LB and BHI agar into Petri dishes respectively for *E.coli* and *S. aureus* at room temperature. The two microbial strains were cultured and checked to

reach a density of 1×10^5 CFU/ml by McFarland method. Consequently, 100 µl of bacteria suspension was spread evenly on the surface of solidified nutrient agar with a dry swab, followed by placing sterilized disk specimens (6 mm diameter) onto the agar dishes. The test was conducted in an incubator with a humidified atmosphere of 5% CO_2 and 95% air at 37 °C for 18 h. The inhibition zone of bacterial growth for each specimen was measured with a metric ruler with millimeter calibration. Six samples of each nanocomposite were used for the tests. Sterile paper disk (6 mm diameter) impregnated with silver nitrate solution was used as control.

Oeteoblastic cell cultivation

Human osteoblast cell line Saos-2 was cultured in Dulbecco's Modified Eagle Medium (DMEM; Thermo Scientific) with 10% fetal bovine serum, 100 mg/ml of streptomycin and 100 U/ml of penicillin. Disk specimens (5 mm diameter) were rinsed with 70% ethanol and PBS solution prior to cell seeding. They were then placed into 96-well plates followed by seeding with 100 µl cell suspension containing 1×10^4 cells per well. These plates were placed in an incubator at 37°C with humidified atmosphere of 95% air and 5% CO_2 for 2 and 4 days. By the end of selected time interval, the specimens were taken out from the wells and rinsed with PBS solution twice to remove unattached cells, then fixed with 10% formaldehyde solution and dehydrated in a series of ethanol solutions (30, 50, 70, 90, 100 vol.%) and critical point drying. Following drying, they were deposited with a thin gold film for SEM observations (Jeol JSM-820).

Cytotoxicity test

The proliferation of osteoblasts on the composite specimens was assessed using 3-(4,5-dimethylthiazol-2-yl)-2,5-diphenyltetrazolium bromide (MTT) assay in 96-well plates. The MTT assay is colorimetric method for evaluating the number of viable cells. A cell suspension with 10^4 cells per well was introduced to cultured plates with and without samples, and incubated in a humidified atmosphere of 5% carbon dioxide in air at 37 °C for 1, 2 and 4 days. The culture medium was refreshed every two days. After the prescribed time, the medium was aspirated, then 10 µL of MTT solution was added to each well and incubated for 4 h for at 37 °C to yield insoluble formazan crystals. The formazan was then dissolved in 10% sodium dodecyl sulfate (SDS) /0.01 M hydrochloric acid (100 µL). The absorbance of dissolved formazan was quantified spectrophotometrically at a wavelength of 570 nm using a multimode detector (Beckman Coulter DTX 880), with a reference wavelength of 640 nm. Wells with MTT and DMEM were used as negative control. The cell viability was evaluated by comparing the absorbance of osteoblastic cells cultured on the nanocomposites with that of cells seeded on pure PLA. Eight samples of each nanocomposite were used for the test, and the results were expressed in terms of mean ± standard deviation (SD).

Biomineralization test

The bioactivity of the PLA/18%nHA-Ag hybrid system was assessed by dipping them into a SBF solution. This solution was made according to the Kokubo practice by dissolving required amounts of chemical reagents to give desired ion concentrations: Na^+ (142 mM), K^+ (5 mM), Ca^{2+} (2.5 mM), Mg^{2+} (1.5 mM), Cl^- (147.8 mM), HCO_3^- (4.2 mM), HPO_4^- (1 mM) and SO_4^{2-} (0.5 mM). It was buffered to pH of 7.4 using tris-(hydroxymethyl, aminomethane and 1M HCl at 37 ºC.[56] The composite specimens were dipped in SBF at 37 °C for 21 day. After immersion, the specimens were removed from the solution, rinsed with distilled water, dried, and then examined in SEM.

Results and discussion

Structure and morphology

Figure 2 shows the X-ray diffraction patterns of binary PLA/18% nHA and ternary PLA/nHA-Ag nanocomposites. PLA displays an intense diffraction peak at 2θ = 16.6° and small peak at 2θ = 18.96°. The XRD pattern of PLA/18% nHA nanocomposite shows the presence of both PLA and nHA diffraction peaks. The nHA peaks at 26.0°, 28.3°, 29.0° 31.9°, 33.0°, 34.2°, 40.7°, 46.7° and 49.4° can be assigned to the (002), (102), (210), (211), (112), (300), (310), (222) and (213) reflections respectively according to the Joint

Committee on Powder Diffraction Standards for hydroxyapatite (JCPDS No.09-0432). For hybrid PLA/nHA-Ag nanocomposites, additional Ag peaks at 38.18° and 44.3° can be readily seen. These two Ag peaks correspond to the (111) and (200) reflections, and their intensity increases with increasing AgNP content in the polymeric matrix. These results indicate that both nHA and AgNP have been incorporated into the PLA matrix by melt-mixing. Figs. 3a-b show representative SEM images of PLA/18% nHA and ternary PLA/18%nHA-6%Ag nanocomposites. Both nHA and Ag fillers are evenly dispersed in the polymer matrix of these composites.
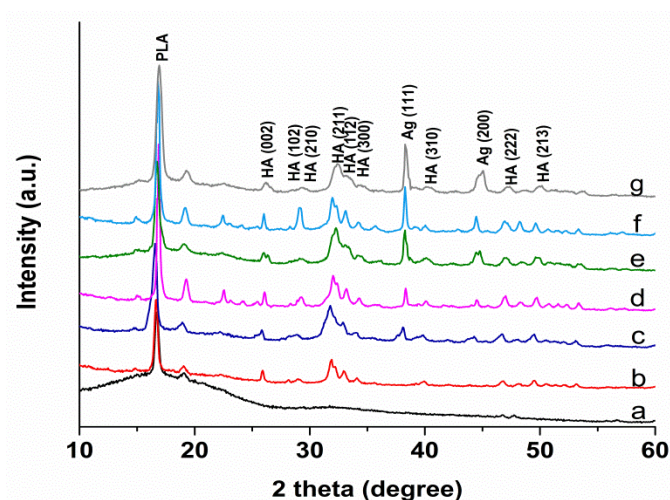
Figure 2. XRD patterns of (a) PLA, (b) PLA/18% nHA, (c) PLA/18% nHA-2% Ag, (d) PLA/18% nHA-6% Ag, (e) PLA/18% nHA-10% Ag, (f) PLA/18% nHA-18% Ag and (g) PLA/18% nHA-25% Ag samples
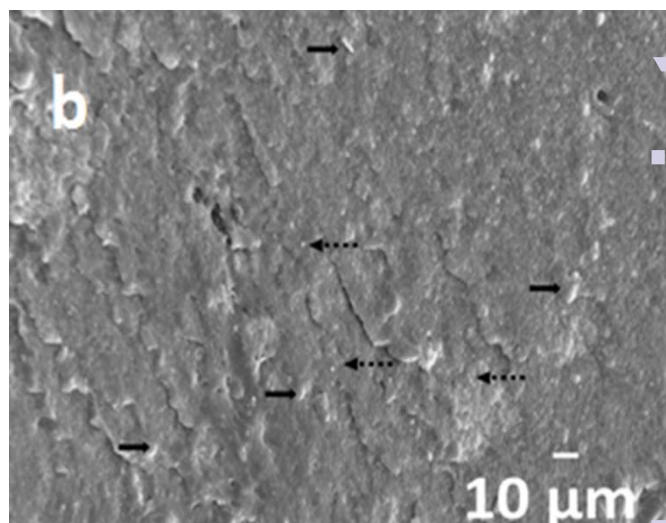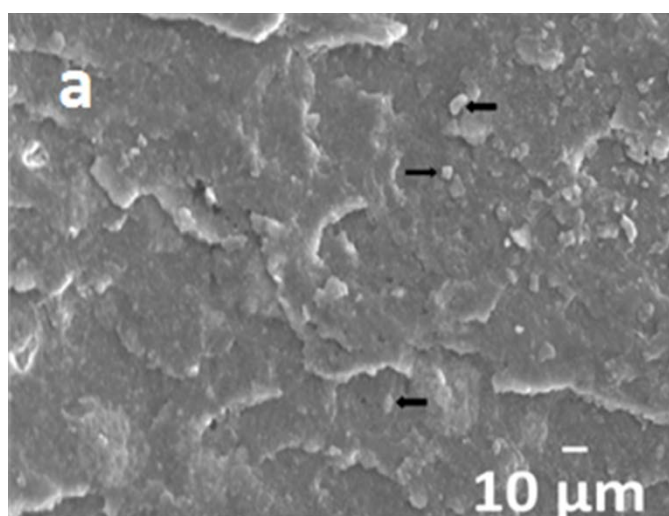

Figure 3. SEM images of cryo-fractured (a) PLA/18% nHA and (b) PLA/18% nHA-6%Ag composites. Solid arrow: nHA and dash arrow: AgNP

Degradation behavior

Figure 4 shows the weight loss vs time for binary PLA/18%nHA and ternary PLA/nHA-Ag nanocomposites immersed in the PBS solution at 37 °C for different time periods. Apparently, PLA shows negligible weight loss after 50 days immersion. However, PLA/18%nHA composite degrades continuously with immersion time. This implies that the nHA filler affects degradation behavior of PLA by increasing its hydrophilicity and water uptake of the polymer matrix. Recently, Delabarte et al. attributed the enhanced degradation rate of PLA/10%nHA in aqueous NaOH at 50 °C to hydrophilicity of nHA having hydroxyl group in its chemical structure.[57] From Fig. 4, the weight loss of PLA/18% nHA nanocomposite can be further increased by adding 18-25 wt% AgNPs. This demonstrates that AgNPs also facilitate PLA disintegration in PBS.

The degradation of PLA is associated with hydrolysis of its ester bonds, catalyzed by the ends of carboxylic chains that are produced during the ester hydrolysis. The cleavage of ester bonds then releases lactic acid. As recognized, metals release ions upon reacting with water. Water molecules form a sphere around a metal ion and hence metal become hydrated.[59,60] In this respect, metal ions form strong bonds with water molecules, and the strength of metal-to-water bond increases with decreasing size. AgNPs with large

surface-to volume ratio that disperse in the PLA matrix surface absorb higher amount of water, promoting hydrolytic scission of ester bonds of PLA largely. Huang et al. indicated that AgNPs react with the oxygen species of the ester group of poly(viny acetate); the acetate groups of the polymer backbone hydrolyze to form hydroxyl species.[61] The resultant metal-containing polymer became more hydrophilic in an aqueous medium. Very recently, Tran et al. reported that the hydrophobic polycaprolactone (PCL) became more hydrophilic after the incorporation of AgNPs.[62]
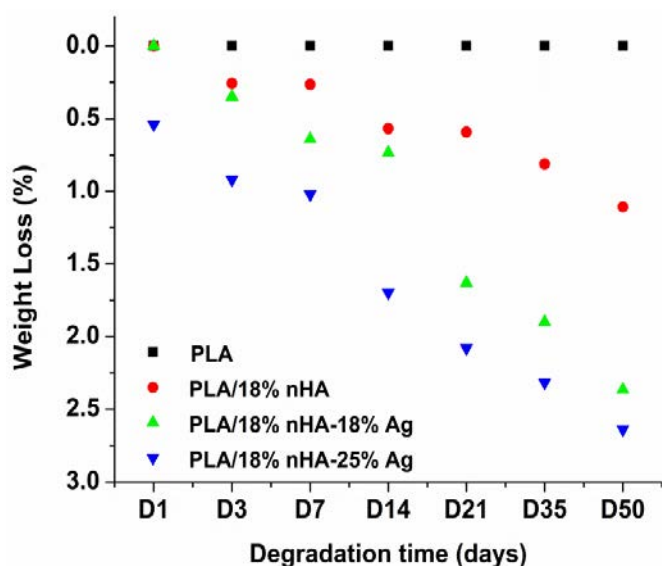

Figure 4. Weight loss vs immersion time for PLA, PLA/18% nHA, PLA/18% nHA-18% Ag and PLA/18% nHA-25% Ag specimens exposed to PBS solution at 37 °C

Figure 5 shows typical SEM image of PLA/18%nHA-25%Ag nanocomposite exposed to the PBS solution for 21 day. Numerous voids can be seen on the specimen surface upon exposure to the solution. Moreover, degradation of the nanocomposite occurs preferentially at the filler-matrix interfaces as indicated by black arrows in the micrograph. Very recently, Wang et al. indicated that the hydrophilicity of Ag-TiO$_2$ films increased with silver content.[63] The best molar ratio of Ag in the Ag-TiO$_2$ films was 1% based on contact angle tests.
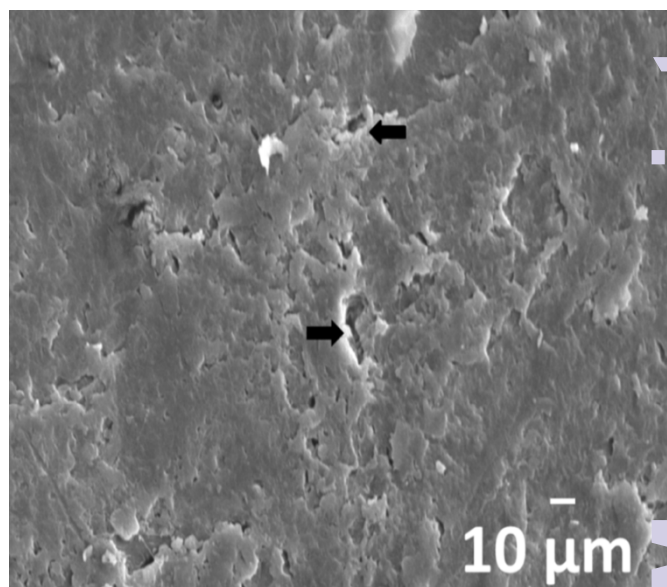

Figure 5. SEM micrograph of PLA/18% nHA-25% Ag nanocomposite after 21 day exposure to PBS solution at 37 °C
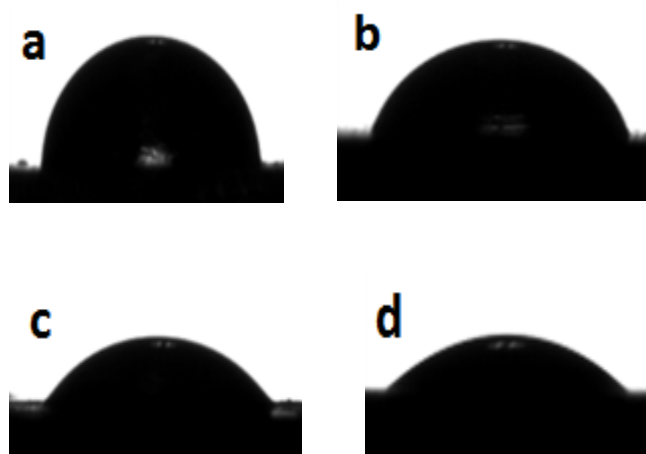

Figure 6. Representative appearances of water contact angles on (a) PLA, (b) PLA/18% nHA, (c) PLA/18% nHA-18% Ag and (d) PLA/18% nHA-25% Ag specimens

In this regard, we have carried out water contact angle tests for PLA and its nanocomposites for assessing hydrophylicity (Fig. 6 and Table 2). It can be seen that PLA exhibits the largest water contact angle of 88.84°, but the incorporation of 18% nHA into PLA reduces the angle to 80.90°. By adding 18-25 wt% AgNPs to the PLA/18%nHA, the contact angle reduces significantly. Therefore, the contact angle results agree reasonably with the weight loss

measurements as shown in Fig. 4. As recognized, PLA generally degrades slowly in-vitro and in-vivo into lactic acid monomers. Our results clearly indicate that its degradation rate can be tailored by the filler components, i.e. nHA and AgNPs in which the latter being more effective.

Table 2. Water contact angle values on PLA and its nanocomposites

Sample	Contact angle, degree
PLA	88.84 ± 5.00
PLA/18% nHA	80.90 ± 2.21
PLA/18% nHA – 2% Ag	77.38 ± 2.50
PLA/18% nHA – 6% Ag	67.38 ± 4.55
PLA/18% nHA – 10% Ag	60.66 ± 3.24
PLA/18% nHA – 18% Ag	48.80 ± 4.60
PLA/18% nHA – 25% Ag	33.56 ± 5.30

Antibacterial Activity

As aforementioned, silver ions released from silver-based materials play an important role in bactericidal activity. Fig. 7 displays the concentration of Ag^+ ion detected in distilled water by immersing PLA/18%nHA-Ag hybrids for 2 to 50 days at 37 °C. For the PLA/18% nHA-2Ag and PLA/18% nHA-6%Ag hybrids, the amount of Ag^+ release is relatively slow at 2 to 7 day, and it becomes faster at 14 day and above. However, larger amounts of Ag^+ ions are released from the PLA/18% nHA-10%Ag and PLA/18% nHA-18%Ag hybrids at 4-7 day periods compared with the hybrids having 2% and 6% Ag. Silver nanoparticles release ions quite effectively because of their large specific surface area. Further, the concentration of Ag^+ release increases with increasing time of immersion (≥ 14 day) due to the polymer degradation. This behavior is more pronounced for the PLA/18% nHA-25%Ag hybrid.
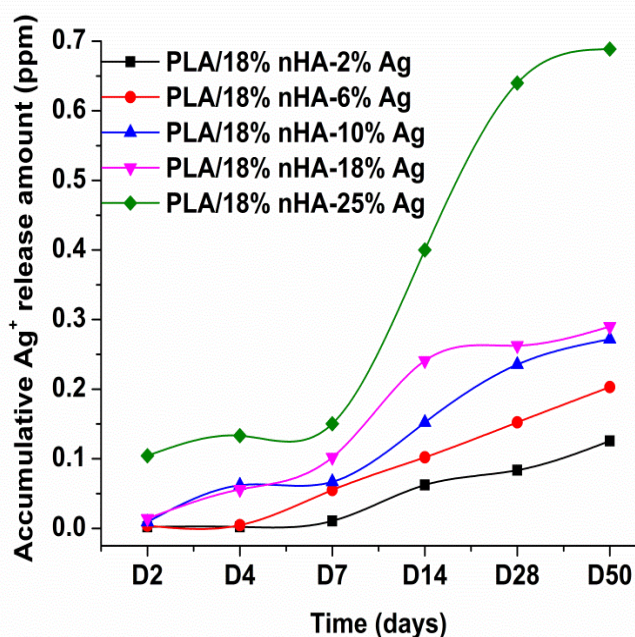

Figure 7. Ag^+ release profiles of PLA/18% nHA-%Ag hybrids containing various AgNP contents after different immersion times in distilled water at 37 °C

Figures 8 and 9 are the disk diffusion test results of PLA and its nanocomposites showing their antibacterial activity against E. coli and S. aureus, respectively. Values of inhibition zones are listed in Table 3. Zone of inhibition reflects the resistance of tested samples against E. coli and S. aureus strains. Silver free PLA and PLA/18% nHA specimens display no inhibition zone to E. coli and S. aureus, i.e. no antibacterial activity. The PLA/18%nHA-Ag system shows strong antibacterial resistance against E. coli. The inhibition zone of PLA/18%-Ag system against E. coli increases with increasing AgNP content. Thus silver nanofillers effectively inhibit the growth of E. coli on agars. The high bactericidal activity is apparently due to the silver cations released from AgNPs that act as reservoirs for the Ag^+ bactericidal agent. In contrast, gram-positive S. aureus strain is more resistant to AgNPs. Only the PLA/18%nHA-18%Ag and PLA/18%nHA-25%Ag hybrids show clear inhibition zones against S. aureus (Figs. 9a-b and Table 3).
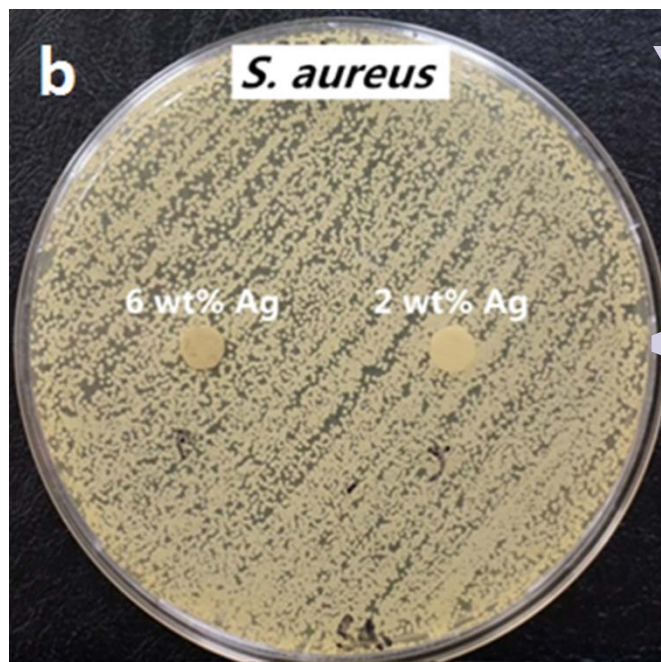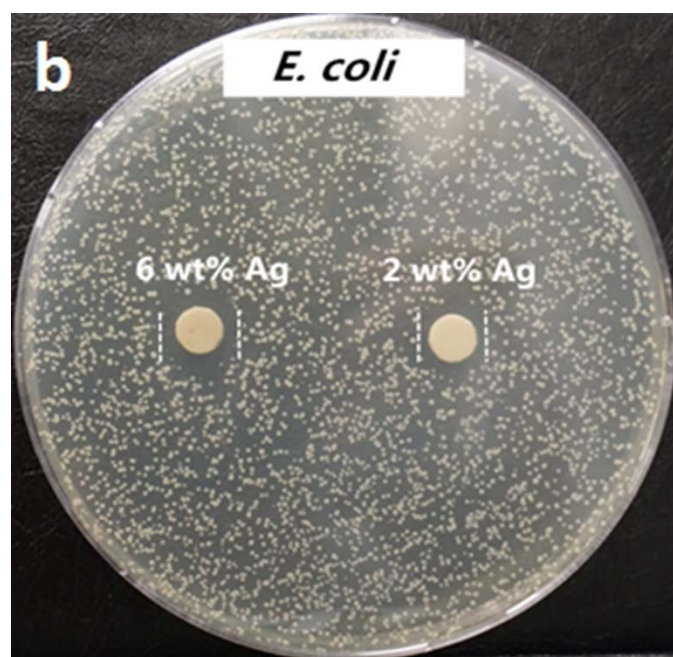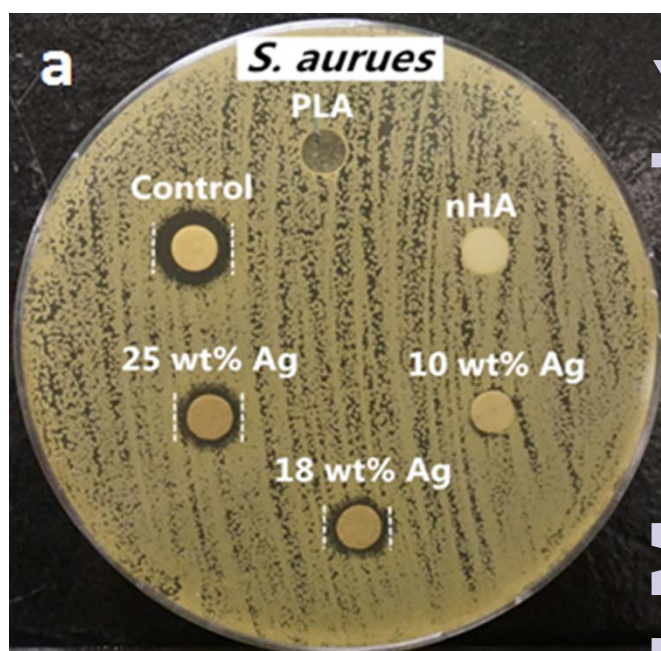
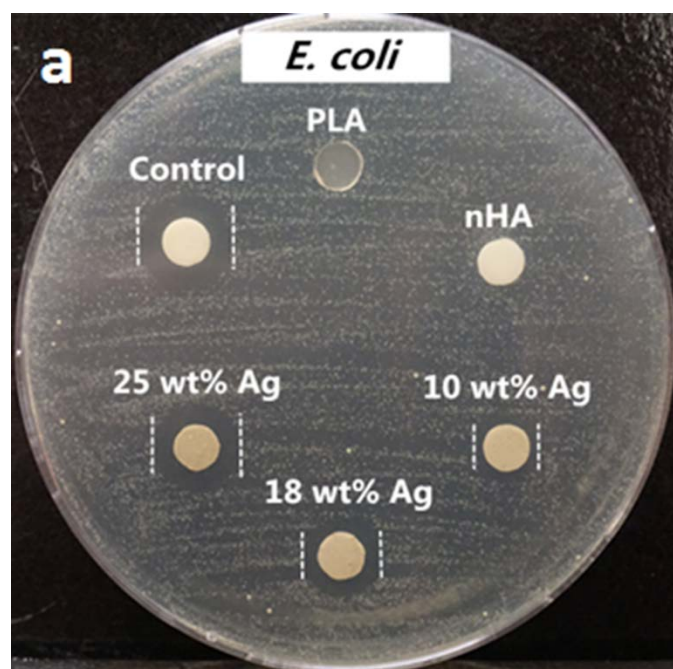**Figure 8.** Photographs of agar plates containing : (a) control (AgNO$_3$), PLA, PLA/18%nHA, PLA/18% nHA-10% Ag, PLA/18% nHA-18% Ag and PLA/18% nHA-25% Ag samples, and (b) PLA/18% nHA-2% Ag and PLA/18% nHA-6% Ag hybrids against E. coli

Figure 9. Photographs of agar plates containing: (a) control (AgNO$_3$), PLA, PLA/18%nHA, PLA/18% nHA-10% Ag, PLA/18% nHA-18% Ag and PLA/18% nHA-25% Ag samples, and (b) PLA/18% nHA-2% Ag and PLA/18% nHA-6% Ag hybrids against S. aureus

Table 3. Average inhibition zone (mm) for AgNO$_3$ control, PLA, PLA/18 wt% nHA, and PLA/18 wt% nHA/Ag with 10, 18 and 25 wt% Ag contents

Sample	E.coli	S. Aureus
AgNO$_3$ Control	12.60±1.10	10.60±0.41
PLA	---	---
PLA/18% nHA	---	---
PLA/18% nHA – 2% Ag	7.52±0.44	---
PLA/18% nHA – 6% Ag	8.62±0.21	---
PLA/18% nHA – 10% Ag	8.70 ±0.80	---
PLA/18% nHA – 18% Ag	10.10±0.60	8.11 ± 0.20
PLA/18% nHA – 25% Ag	11.10±0.60	8.74 ± 0.13

As recognized, cell membrane structures of the gram-positive and gram-negative bacteria are different, but they have a negatively surface charge. Gram-positive bacteria have a thick external layer of peptidoglycan together with teichoic and lipoteichoic acids lying on the plasma membrane. Teichoic acids are water-soluble polymers of polyol phosphates. Their cell structure is negatively charged due to the presence of phosphate, carboxyl and amino groups.[64] Thick peptidoglycan layer with a more rigid structure causes difficult penetration of AgNPs. In contrast, gram-negative bacteria have an external lipopolysaccharide followed by a thin layer of peptidoglycan and plasma membrane. The inner core region of polysaccharide contains heptose residues which are often substituted by phosphate, pyrophosphate or diphosphoethano-lamine.[65] Price et al. indicated that the outer cell layer of E.coli composed of lipid A-containing lipopolysaccharide and glycerophospholipid. Lipid A contains two phosphate groups in each glycosaminoglycan.[66] Therefore, cell membranes with negatively charged can attract positively charged Ag$^+$ ions from silver-containing hybrids through electrostatic interactions, thereby deactivating cellular enzymes, causing disruption in membrane integrity. Furthermore, Ag$^+$ ion can interact with thiol groups in protein, promoting the release of oxygen reactive species. This causes damage to proteins and DNA, resulting in cell death.[67,68] In general, Ag$^+$ ions are more active and effective against E. coli than gram-positive S. aureus since the membrane

of E. coli contains a higher proportion of negatively charged phosphate groups. Kim et al. reported that low AgNP concentrations inhibit the growth of E. coli effectively, whereas the growth-inhibitory effect of AgNPs on S. aureus was mild.[69]

In this study, antibacterial efficacy of PLA/18% nHA-Ag system against E. coli and S. aureus depends greatly on the AgNP loading levels. It is worth-noting that the polymer matrix material also plays an important role in bactericidal activity. As aforementioned, the incorporation of nHA and AgNPs into PLA enhances its hydrophilicity (Fig. 6). Enhanced hydrophilicity facilitates the degradation and disintegration of PLA in aqueous medium, thereby exposing AgNPs embedded in the PLA matrix to the environment and releasing silver ions for antibacterial activity. To substantiate this, we have melt-mixed polyvinylidene fluoride (PVDF) with 5-25 wt% AgNPs. PVDF is a hydrophobic thermoplastic having good piezoelectricity, thus showing extensive applications in biosensor, biomedical and pharmaceutical sectors. Silver ion release measurement confirms the absence of Ag$^+$ ions from melt-compounded PVDF/Ag composites upon immersion in distilled water for prolonged times. This implies that non-degradable PVDF matrix cannot expose Ag nanofillers effectively in aqueous medium, i.e. silver nanofillers unable to release Ag$^+$ ions for killing bacteria. As a result, agar disk diffusion tests show no inhibition zones for both E. coli and S. aureus strains.

Bioactivity and cytotoxicity

Figures 10a-b and 11a-b are the SEM micrographs of PLA/18%nHA and PLA/18%nHA-2%Ag nanocomposites after seeding with osteoblasts for 2 and 4 days, respectively. The cells anchor tightly on the surfaces of these specimens after 2 day cultivation. The cells grow and spread flatly on the surface, and many neighbor cells link with each other through cytoplasmic extension after 4 day cultivation. The nHA fillers provide effective sites and support for the adhesion of osteoblasts. Bioinert PLA is ineffective for the adhesion and attachment of bone cells. Thus it is necessary to add nHA with good bioactivity and biocompatibility to PLA. The nHA content needed for achieving this purpose is 18-20 wt% from our previous studies.[70,71]
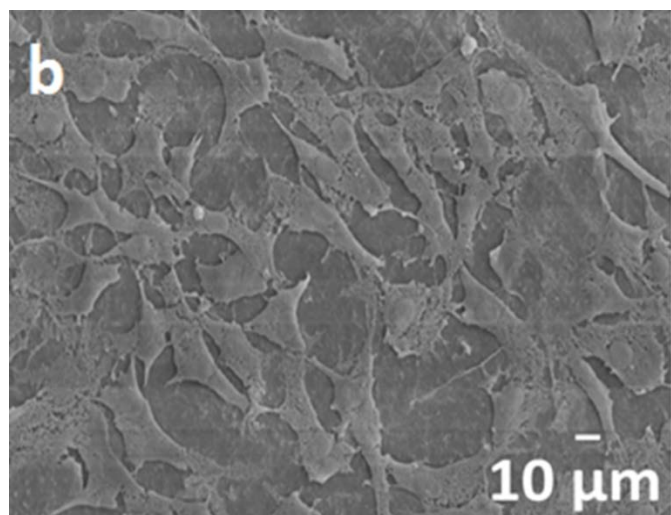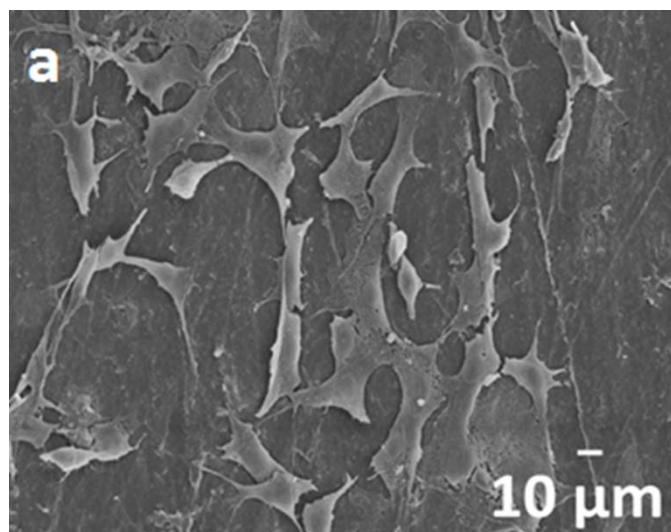
Figure 11. SEM images of osteoblasts cultured on PLA/18%nHA-2%Ag hybrid for (a) 2 and (b) 4 day
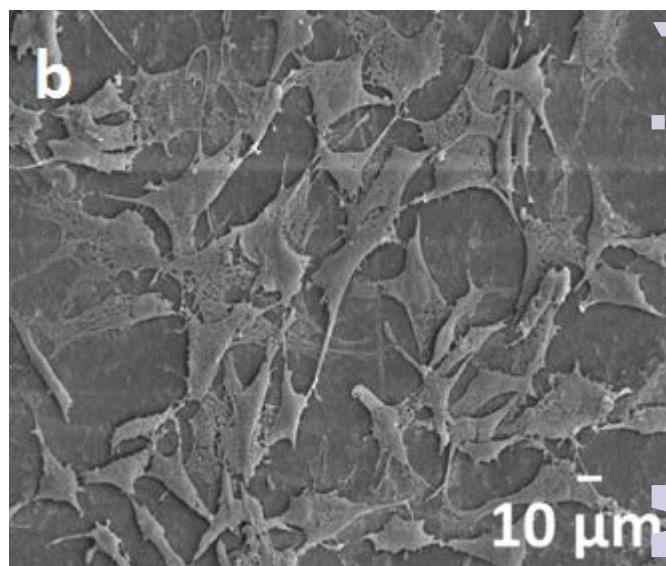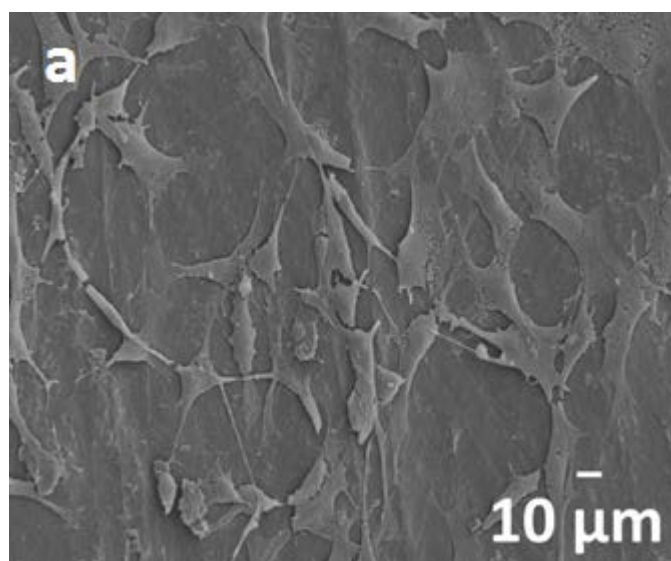

Figure 10. SEM images of osteoblasts cultured on PLA/18%nHA nanocomposite for (a) 2 and (b) 4 day

Medical devices for successful clinical implantations and applications should balance their antibacterial activity and cytocompatibility properly. Although silver nanofillers of the PLA/18%nHA-Ag system exhibit bactericidal effect to E. coli at 2-25 wt% Ag loadings, and to S. aureus at high Ag loading levels (18 and 25 wt%), they may have cytotoxicity to osteoblasts. The cytotoxicity of binary PLA/18% nHA composite and ternary PLA/18% nHA-Ag hybrids can be determined with the MTT assay. This assay is commonly used to assess mitochondria activity of the cells. Fig. 12 shows the cellular viability of PLA and its nanocomposites cultivated with osteoblasts for 1, 2 and 4 days. After 4 day incubation, binary PLA/18% nHA and ternary PLA/18% nHA-2%Ag specimens show improved cell growth behavior compared with PLA. Cellular viability of the PLA/18%nHA-6%Ag and PLA/18%nHA-10%Ag hybrids decreases slightly due to the toxicity of AgNPs. Moreover, cellular viability of the hybrids with high AgNP loadings, i.e., PLA/18%nHA-18%Ag and PLA/18%nHA-25%Ag reduces significantly. This demonstrates that high AgNP contents inhibit the proliferation of osteoblasts owing to the cytotoxicity of silver nanoparticles. From these results, it is necessary to add adequate AgNP filler contents in the PLA/18% nHA composite to reduce

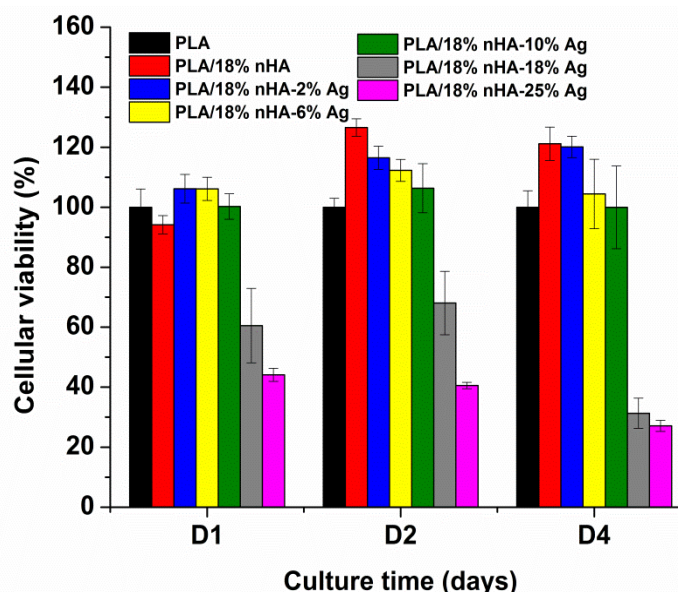bacteria contamination and to minimize bone tissue cytotoxicity.

Figure 12. Cell viability of osteoblasts grown on PLA and its nanocomposites after seeding for 1, 2 and 4 day. The viability of cells on PLA was set at 100%.

Apart from cell cultivation and MTT tests, the effect of Ag additions on biomineralization of the PLA-18%nHA composite is also investigated. For successful osteointegration, the hybrid composites should also exhibit enhanced biomineralization capability in addition to good biocompatibility. An evaluation of the bioactive behavior of the composites is done by immersing them in simulated body fluid. Figs. 13(a) and (b) are representative SEM micrographs showing surface morphologies of the PLA/18% nHA and PLA/18% nHA-2%Ag specimens after dipping 21 day in the SBF solution, respectively. The whole surfaces of both specimens are almost covered with the apatite layer. The EDS spectra of this layer (insets) reveal the presence of calcium and phosphorus. The formation of apatite layer is associated with enhanced diffusion, adsorption and precipitation of Ca^{2+} ions from the SBF solution, and subsequent electrostatic attraction between Ca^{2+} ions with the OH^- and PO_4^{3-} groups of nHA filler. Figs. 14(a)-(c) show representative SEM cross-sectional images of PLA/18% nHA, PLA/18% nHA-10%Ag PLA/18% nHA-25%Ag composites after 21 day immersion.

Apparently, a dense apatite layer can be fully developed on the surfaces of binary PLA/18% nHA and ternary PLA/18%nHA-Ag hybrids by dipping in a SBF solution for 21 day. Thus Ag additions to the PLA/18%nHA composite do not impair its biomineralization efficiency.
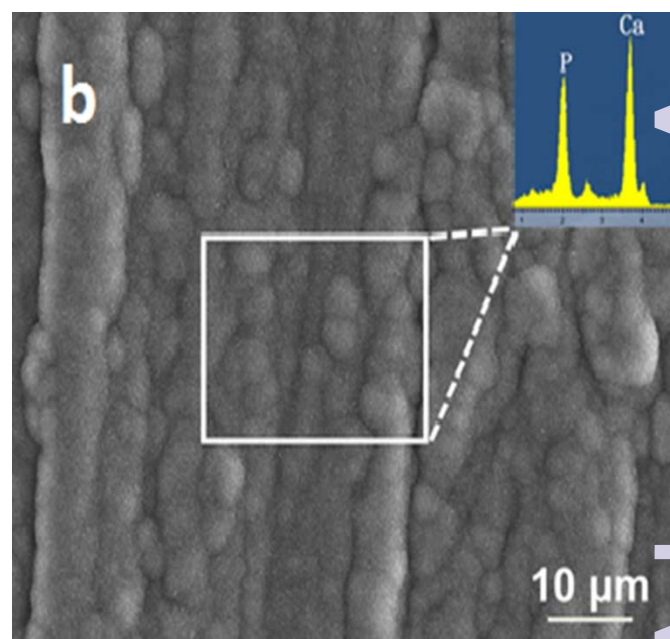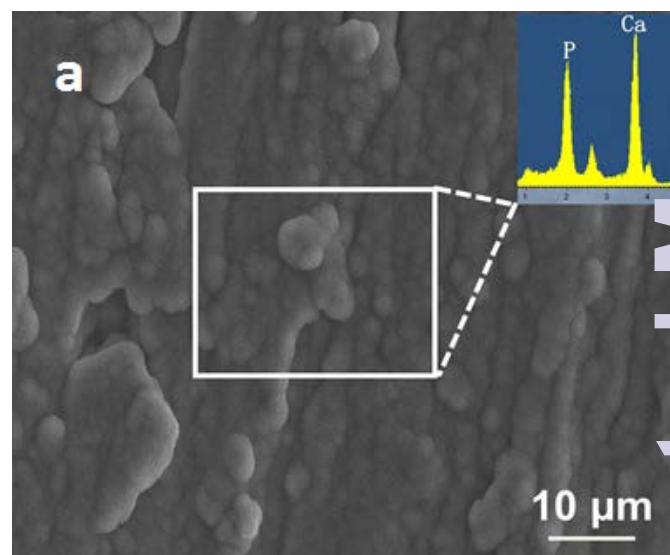

Figure 13. SEM micrographs showing apatite layer formed on the surfaces of (a) PLA/18% nHA and (b) PLA/18%nHA-2%Ag nanocomposites immersed in SBF solution for 21 day.
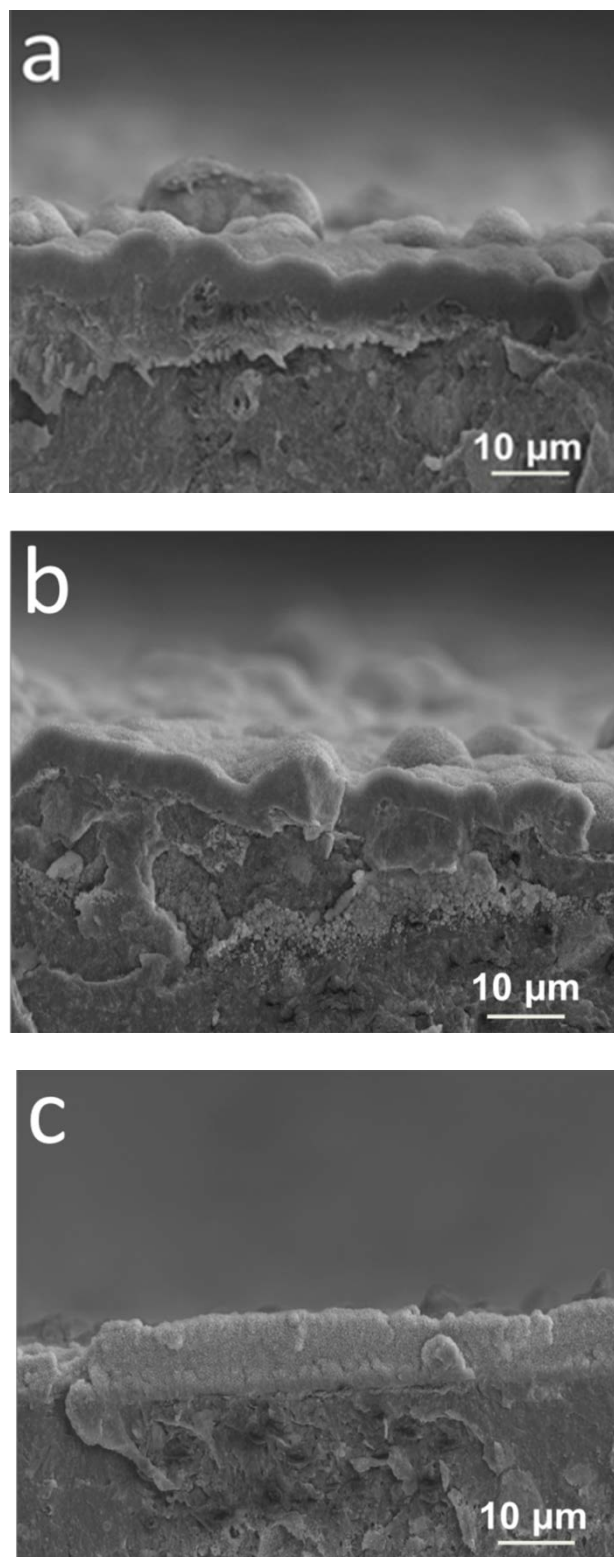
Figure 14. SEM cross-sectional micrographs showing apatite surface layer formed on (a PLA/18% nHA, (b) PLA/18% nHA-10%Ag and (c) PLA/18% nHA-25%Ag nanocomposites immersed in SBF solution for 21 day

Conclusions

In this article, we presented the fabrication of bulk PLA/18%nHA-Ag hybrids with different AgNP loadings using melt-compounding process. The effects of AgNP additions on the biodegradation, antibacterial activity and cytotoxicity of PLA.18%nHA composite were studied. Weight-loss and water contact angle tests showed that the nHA and Ag nanofillers increase the degradation rate and hydrophilicity of PLA respectively, but AgNPs being more effective than nHA. Further, the degradation rate of PLA/18%nHA-Ag hybrids can be tailored by monitoring AgNP contents. Dis diffusion test results demonstrated that all PLA/18%nHA-Ag hybrids show high bactericidal activity against E. coli and moderate activity against S. aureus. MTT test results revealed that high AgNP contents (18 and 25 wt%) inhibit the proliferation of osteoblasts. However, composite hybrids with low loading Ag levels (2 and 6 wt%) showed good biocompatibility over PLA. Finally, a dense apatite layer can be fully developed on the surfaces of binary PLA/18% nHA and ternary PLA/18%nHA-Ag hybrids by dipping in a SBF solution for 21 day, demonstrating good bioactivity.

References

1　B. L. Seal, T. C. Otero and A. Panitch, *Mater. Sci. Eng. R,* 2001*,* **34***,* 147-240.

2　D. G. Barrett and M. N. Yousaf, *Soft Matter*, 2010, **6**, 5026– 5036.

3　S. C. Tjong and Y. Z. Meng, *Eur. Polym. J.*, 2000, **36**, 123–129.

4　Y. Z. Meng, S. C. Tjong, A. S. Hay and S. J. Wang, *J. Polym. Sci. Part A-Polym.Chem.*, 2001, **39**, 3218-3226.

5　X. H. Li, S. C. Tjong, Y. Z. Meng and Q. Zhu, *J. Polym. Sci. Part B- Polym. Phys*., 2003, **41**, 1806-1813.

6　Y. Z. Meng and S. C. Tjong, *Polymer*, 1998, **39**, 99-107.

7　Y. Z. Meng, A. S. Hay, X. G. Jian and S. C. Tjong, *J. Appl. Polym. Sci.*, 1998, **68**, 137-143.

8　A. Terriza, J. I. Vilches-Perez, J. L. Gonzalez-Caballero, E. de la Orden, F. Yubero, A. Barranco, A. R. Gonzalez-Elipe, J. Vilches

and M. Salido, *Materials*, 2014, **7**, 1687-1708.

9 M. Singhvi and D. Gokhale, *RSC Adv*., 2013, **3**, 13558-13568.

10 R. Ferrari, C. M. Pecoraro, G. Storti and D. Moscatelli. *RSC Adv*., 2014, **4**, 12795-12804.

11 J. B. Zeng, K. A. Li and A. K. Du, *RSC Adv*., 2015, **5**, 32546-32565.

12 W. J. Hendrikson, J. Rouwkema, C. A. van Blitterswijk and L. Moron, *RSC Adv*., 2015, **5**, 54510-54516.

13 S. P. Ju, W. C. Huang and C. C. Chen, *RSC Adv*., 2014, **4**, 35862-35867.

14 K. Rezwan, Q.Z. Chen, J.J. Blaker and A.R. Boccaccini, *Biomaterials*, 2006, **27**, 3413–3431.

15 J. Viljanen, J. Kinnunen, S. Bondestam, A. Majola, P. Rokkanen and P. Tormala, *Biomaterials*, 1995, **16**, 1353-1358.

16 L. C. Du, Y. Z. Meng, S. J. Wang and S. C. Tjong, *J. Appl. Polym. Sci.*, 2004, **92**, 1840-1846.

17 S. C. Tjong and Y. Z. Meng, *Polymer*, 1997, **38**, 4609-4615.

18 S. C. Tjong, S. L. Liu and R. K. Y. Li, *J. Mater. Sci.*, 1996, **31**, 479-484.

19 K. L. Fung, R. K. Y. Li and S. C. Tjong, *J. Appl. Polym. Sci.*, 2002, **85**, 169-176.

20 S. C. Tjong and Y. Z. Meng, *Polymer*, 1998, **39**, 5461-5466.

21 X. L. Xie, B.G. Li, Z.R. Pan, R.K.Y. Li and S.C. Tjong, *J. Appl. Polym. Sci.*, 2001, **80**, 2105-2112.

22 J. Huang, L. Disilvio, M. Wang, K. E. Tanner and W. Bonfield, *J. Mater. Sci.: Mater. Med.*, 1997, **8**, 775-779.

23 M. S. Abu Bakar, P. Cheang and K. A. Khor, *Compos. Sci. Technol.*, 2003, **63**, 421-425.

24 L. Shor, S. Guceri, X. Wen, M. Gandhi and W. Sun, *Biomaterials*, 2007, **28**, 5291-5297.

25 Y. Shikinami and M. Okuno, *Biomaterials*, 1999, **20**, 859-877.

26 S. C. Tjong, Carbon Nanotube Reinforced Composites: Metal and Ceramic Matrices, Wiley-VCH, Winheim, Germany, 2009, 1-228.

27 S. C. Tjong and S. P. Bao, *Compos. Sci. Technol.*, 2007, **67**, 314-323.

28 Y. C. Li, S. C. Tjong and R. K. Y. Li, *Synth. Met*., 2010, **160**, 1912-1919.

29 S. C. Tjong and G. D. Liang, *Mater. Chem. Phys*., 2006, **100**, 1-5.

30 R. A. Hule and D. J. Pochan, *MRS Bull.* 2007, **32**, 354-358.

31 P. A. Tran, L. Sarin, R. H. Hurt and T. J. Webster, *J. Mater*. *Chem.*, 2009, **19**, 2653-2659.

32 C.I.R. Boissard, P. E. Bourban, A.E. Tami, M. Alini, D. Eglin, *Acta Biomater*., 2009, **5**, 3316-3327.

33 A. Ronca, L. Ambrosio, D.W. Grijpma, *Acta Biomater*., 2013, 9, 5989-5996.

34 J. C. Fricain, S. Schlaubitz, C. Le Visage, I. Arnault, S. M. Derkaoui, R. Siadous, S. Catros, C. Lalande, R.Bareille, M.Renard, Fabre, S. Cornet, M. Durand, A. Leonard, N Sahraoui, D. Letourneur and J Amédée, *Biomaterial*s, 2013, **34**, 2947-2959.

35 B. Basu, S. K. Swain and D. Sarkar, *RSC Adv.*, 2013,**3**, 14622-14633.

36 J. Suganuma and H. Alexander, *J. Appl. Biomater*., 1993, **4**, 13-27.

37 H. Y. Li and J. Chang, *Compos. Sci. Technol*., 2005, **65**, 2226-2232.

38 D. Campoccia, L. Montanaro and C. R. Arciola, *Biomaterials*, 2006, **27**, 2331-2339.

39 J. F. Hernandez-Sierra, F. Ruiz, D. C. Pena, F. Martinez-Gutierrez, A. E. Martinez, A. Guillen, H. Tapia-perez and G. M. Castanon, *Nanomedicine*, 2008, **4**, 237-240.

40 L. Grenho, F. J. Monteiro and M. P. Ferraz, *J. Biomed. Mater. Res. A.*, 2014, **102**, 3726-3733.

41 R. Kumar and H. Munstedt, *Biomaterials*, 2005, **26**, 2081-2088.

42 E. C. Dreaden, A.M. Alkilany, X. Huang, C. J. Murphy and M. A. El-Sayed, *Chem. Soc. Rev.,* 2012, **41**, 2740-2779.

43 J. T. Seil and T. J. Webster, *Acta Biomater*. 2011, **7**, 2579-2584.

44 I. Sondi and B. Salopek-Sondi, *J. Colloid Interface Sci*., 2004, **275**, 177-182.

45 S. Agnihotri, S. Mukherjiabc and S. Mukherji, *Nanoscale*, 2013, **5**, 7328-7340.

46 C. Damm, H. Munstedt and A. Rosch, *Mater. Chem. Phys*., 2008, **108**, 61-66.

47 W. Chen, Y. Liu, H. S. Courtney, M. Bettenga, C.M. Agrawal, J.D. Bumgardner and J. L. Ong, *Biomaterials*,2005, **27**, 5511-5517.

48 S. Eraković, A. Janković, D. Veljović,, E, Palcevskis, M. Mitrić and T. Stevanović, *J. Phys. Chem. B*, 2012, 117, 1633-1643.

49 S. Erakovic, A.Jankovic , G. C. P. Tsui , C. Y. Tang, V. Miskovic-Stankovic and T. Stevanovic, *Int. J. Mol. Sci,.* 2014, **15**, 12294-12322.

50 K. Shameli, M. Bin Ahmad, W. M. Yunus, N. A. Ibrahim, R. A. Rahman, M. Jokar and M. Darroudi, *Int. J. Nanomedicine*, 2010, **5**, 573-579.

51 A. Mostafa, H. Oudadesse, Y. Legal, E. Foad and G. Cathelineau, *Bioceram. Dev. Appl.*, 2011, **1**, ID D101128, 3pp.

52 A. Sobczak-Kupiec, D.Malina1, M. Piatkowski, K. Krupa-`Zuczek1, Z. Wzorek and B. Tyliszczak, *J. Nanosci. Nanotechnol.,* 2012, 12, 9302-9311.

53 ASTM F1635-04: Standard Test Method for *in Vitro* Degradation Testing of Hydrolytically Degradable Polymer Resins and Fabricated Forms for Surgical Implants, 2004.

54 A. W. Bauer, W. M. Kirby, J. C. Sherris and M. Turck, *Am. J. Clin. Pathol.*, 1966, **45**,493–496

55 http://www.microbelibrary.org/component /resource/laboratory-test/3189-kirby-bauer-disk-diffusion-susceptibility-test-protocol

56 T. Kokubo and H. Takadama, *Biomaterials* 2006, **27**, 2907- 2915 .

57 C. Delabarte, C. J. Plummer, P. E. Bourban and J. A. Manson, *Polym. Degr. Stab.*, 2011, **96,** 595-607.

58 I. Armentano, M. Dottori, E. Fortunati, S. Mattioli and J.M. Kenny, *Polym. Degr. Stab.*, 2010, **95**, 2126-2146.

59   S. C. Tjong and E. Yeager, *J. Electrochem. Soc.*, 1981, **128**, 2251-2254.

60 M. Holovko, M. Druchok and T. Bryk, *J. Electroanal. Chem.*, 2005, 582, 50-56.

61 C. J. Huang, D. S. Shieu, W. P. Hsieh and T. C. Chang, *J. Appl. Polym. Sci.,* 2006, **100**, 1457-1464.

62 P. A. Tran, D. M. Hocking, A. J. O'Connor, *Mater. Sci. Eng. C-Mater. Biol. Appl.*, 2015, **47**, 63-69.

63 X. Wang, X. Hou, W. Luang, D. Li and K. Yao, *Appl. Surf. Sci.*, 2012, **258**, 8241-8246.

64 A. van der Wal, W. Norde, A. J. B. Zehnder, and J. Lyklema, *Colloids Surf. B Biointerfaces*, 1997, **9**, 81–100.

65 M. Caroff, D. Karibian, J. M. Cavaillon, N. Haeffner-Cavaillon, *Microbes Infect*. , 2002, **4**, 915-926.

66 N. P. Price, B. Jeyaretnam, R. W. Carlson, J. L. Kadrmas, C. R. Raetz and K. A. Brozek, *Proc. Natl. Acad. Sci. USA*, 1995, **92**, 7352-7356.

67 H. L. Suh, C. C. Chou, D. J. Hung, S. H. Lin, I. C. Pao, J. H. Lin, F. L. Huang , R. X. Dong and J. J. Lin, *Biomaterials*, 2009, **30**, 5979-5987.

68 Z. Hossain and F. Huq, *J. Inorg. Biochem.*, 2002, 91, 398-404.

69 J. S. Kim, E. Kuk, K. N. Yu, J. H. Kim, S. J. Park, H. J. Lee, S. H. Kim, Y. K. Park, Y. H. Park, C. Y. Hwang, Y. S. Lee, D. H. Jeong and M. H. Choo, *Nanomedicine*, 2007, **3**, 95-101.

70 C. Z. Liao, H. M. Wong, K. W. K. Yeung and S. C. Tjong, *Int. J. Nanomedicine*, 2014, 9,1299-1310.

71 C. Z. Liao, H. M. Wong, K. W. K. Yeung and S. C. Tjong, *Mater. Sci. Eng. C-Mater. Biol. Appl.*, 2013, **33**, 1380-1388.